Int J Adv Manuf Technol (2015) 78:1629–1640
DOI 10.1007/s00170-014-6762-y

ORIGINAL ARTICLE

Experiment-based regional characterization of HAZ mechanical properties for laser welding

Chunhua Wei · Jing Zhang · Shanglu Yang · Wu Tao · Fengshun Wu · Weisheng Xia

Received: 8 March 2014 / Accepted: 29 December 2014 / Published online: 13 January 2015

Abstract As for the tailor welded blanks (TWB) of dual-phase steels, heat-affected zone (HAZ) always exhibits significant changes of mechanical properties after experiencing the laser welding process. Hence, the characterization of HAZ mechanical properties is very critical for the accurate forming simulation and service performance of laser-welded blanks. However, it is still difficult to obtain the regional mechanical properties of HAZ because it has a varied transition of microstructures and mechanical properties in a very narrow range (e.g., <1 mm). In this paper, to investigate the regional mechanical properties of HAZ in the laser-welded joints of DP600 steels, an experimental approach was carried out based on the thermal simulation running on the Gleeble machine. The thermal histories of different regions in HAZ during laser welding were simultaneously measured by thermocouples, and then applied for the thermal simulation. The regional characterization of HAZ mechanical properties was realized with the thermal-simulated HAZ specimens. The results show that the thermal histories in weld and HAZ are very sensitive to the distance from the weld centerline, which results in different relevant microstructures and mechanical properties. The tensile strength of HAZ at different locations decreases with increasing distance from the weld centerline, but the elongation has the opposite tendency. The regional mechanical properties of HAZ were also applied to the finite element model of the tensile testing for welded joint by ABAQUS, an elastic-plastic finite element code. And the finite element simulation shows good agreement with the experimental.

Keywords Laser welding · Heat-affected zone · Thermal history · Thermal simulation · Regional mechanical properties

C. Wei · F. Wu · W. Xia (✉)
State Key Laboratory of Materials Processing and Die & Mould Technology, Huazhong University of Science and Technology, Wuhan 430074, People's Republic of China
e-mail: xiawsh@hust.edu.cn

J. Zhang · S. Yang · W. Tao
China Science Lab., GM (China) Investment Co. Ltd, Shanghai 201206, People's Republic of China

1 Introduction

Tailor-welded blanks (TWBs) have been developed to meet the requirements of cost and weight reduction in automotive industry [1, 2]. To predict the forming behavior of TWBs, finite element (FE) method is widely applied to save experimental cost and time. Some researchers assume that the weld zone is a rigid weld line and HAZ is base metal [3–7]. This assumption is based on that weld and HAZ are only a small proportion of the whole TWB, and the models can obtain the reasonable results for mild steels. However, both weld and HAZ are the separate zones, which have different mechanical properties from those of base metal. Especially for the TWBs of advanced high-strength steel (AHSS), their weld and HAZ are sharply different with base metal after enduring welding thermal histories, such as hardened weld and softened HAZ [8–10]. Hence, this assumption is hard to accurately predict the forming behavior [11]. Furthermore, to improve the FE model accuracy [11–16], it is necessary to consider the difference between mechanical properties of weld and HAZ and that of base metal, especially for TWBs of AHSS [17, 18]. Consequently, it is very important to characterize the regional mechanical properties of weld and HAZ.

In addition, experimental methods also have been reported to characterize the mechanical properties of weld and HAZ. One is the thin tensile specimen cut directly from weld and

HAZ to obtain their regional mechanical properties [19–21]. This method assumes that weld and HAZ have homogeneous mechanical properties, which is not the real case for actual weld and HAZ. And it also needs sufficiently large specimens, i.e., wide size weld and HAZ, which is relatively easier for arc welding [20, 21] but rather difficult for laser welding [19].

Another common method is the "rule of mixture," which can calculate the average mechanical properties of weld zone based on the tensile testing of welded joints [21–24]. Although this method can be applied to the relatively narrow weld zone even to laser-welded welds, the characteristic of HAZ region represented by the average properties is still rather coarse. Consequently, to characterize regional strain-stress curves of weld and HAZ, shear test [25], microhardness test [25–28], and indentation test [17, 20, 29] have been adopted. In these methods, the test results are converted to the strain-stress curves based on the empirical formulas, while the formulas need the sufficient experimental verification. To directly measure the regional strain-stress curves of weld and HAZ, digital image correlation (DIC) method has been attempted for friction stir welds [30–34], arc welds [35, 36], and laser-welded welds [37–39] during tensile testing. Since DIC method only can obtain the local strain, the determination of the local stress is still based on the iso-stress assumption in the whole tensile specimen. However, as for the laser-welded joints of AHHS, little plastic deformation will occur at weld and the harder part of HAZ during tensile loading, and thus only a part of whole strain-stress curve can be obtained [8, 9, 40].

Compared with the methods mentioned above, thermal simulation can produce the enlarged HAZ specimen based on the actual thermal history of HAZ. The thermal-simulated specimen has the relatively homogeneous mechanical properties and can be used for the directly test of the mechanical properties of HAZ. This method has been used for arc welding based on the measured thermal histories to study the mechanical properties of HAZ [41, 42]. However, there are still limited reports to apply this method to laser welding. The reasons may due to the following: (1) Compared with arc welding, the rapid heating and cooling process of laser welding is more difficult to be measured and reproduced; (2) The HAZ of laser-welded joint is a very narrow range (e.g., <1 mm) with a varied transition of microstructures and mechanical properties. Therefore, the thermal history measurement and subsequent thermal simulation for different regions in HAZ are necessary but still very challenging.

In this study, thermal histories of different regions in laser-welded HAZ are measured by thermocouples and data acquisition system. Based on these measured thermal histories, thermal simulation running on the Gleeble machine is carried out to obtain thermal-simulated HAZ specimens, and the regional mechanical properties of the resultant HAZ are investigated. Then the FE model of the uni-axial tensile test is developed to validate the mechanical properties of HAZ regions.

2 Experimental

2.1 Materials and laser welding process

Galvanized DP600 steel with a thickness of 0.7 mm is selected as base metal (BM). The main chemical composition and mechanical properties of the base metal are given in Table 1, where YS, UTS, and TEL stand for yield strength, ultimate tensile strength, and total elongation, respectively.

An IPG YLR-4000 laser device was used (wavelength, 1,060 nm; focal length, 250 mm; focal spot diameter, 0.3 mm), and the laser head was mounted on the end arm of an ABB robot. Schematic diagram of laser welding setup is shown in Fig. 1. The DP600 steel sheets were clamped in butt-joint configuration (Fig. 1a). Edge preparation by the finish milling was done before welding process to make sure the gap between the two sheets was smaller than 10 % of the sheet thickness. The detailed setup of laser beam and shielding gas are shown in Fig. 1b. The defocusing distance of laser beam was set at +2.0 mm from the sheet surface. Argon gas was supplied as the shielding gas at a flow rate of 33 L/min.

2.2 Thermal history measurement

Thermal histories were measured by thermocouples and recorded by an eight-channel computer-based data acquisition system (the sampling frequency of 1 k Hz). According to the different peak temperatures scope of weld (higher than the melting point of base metal, 1,530 °C) and HAZ (730–1,530 °C), C-type thermocouples (W5Re-W26Re, the short-time temperature tolerance of 2,310 °C) and K-type thermocouples (Ni-Cr/Ni, the short-time temperature tolerance of 1,350 °C) were selected for the temperature measurement of weld and HAZ, respectively. This case can make the two types of thermocouples both work in their suitable temperature range.

Laser-welding experiments were carried out under various process parameters to obtain the full-penetrated welds with the good surface quality and the cross-section geometry. The laser power and the welding speed were selected as 1.5 kW and 3.0 m/min in this study, respectively. Before the measurement of thermal history, metallographic examination and microhardness testing were both carried out firstly to verify the regions of weld and HAZ. And then micro-holes (the inner diameter of ~0.3 mm and a depth of ~0.3 mm) are drilled in the scope of weld and HAZ to position thermocouples at desired locations. The thermocouples were welded into the micro-holes to ensure the good contact by a thermocouple welding machine, as shown in Fig. 1a. To realize the quick

Table 1 Chemical composition and mechanical properties of DP600 steel

Chemical composition (wt%)									Mechanical properties			
C	Mn	P	Si	Ni	S	Al	Cr	Ti	YS (MPa)	UTS (MPa)	TEL (%)	Microhardness ($HV_{0.2}$)
0.096	1.5	0.015	0.1	0.01	0.01	0.03	0.02	0.01	390	604	29	203

response and accurate positioning, very thin thermocouples (0.1 mm in diameter for C-type and 0.125 mm in diameter for K-type thermocouples) were selected.

2.3 Thermal simulation

Thermal simulation of HAZ was carried out by a Gleeble® 3500 system, and all the specimens were machined into the dimension of 100 mm×30 mm×0.7 mm. The experimental setup and specimen are shown in Fig. 2. The key parameters of the actual thermal histories of laser welding, including heating rate, peak temperature, and cooling rate, were input to the Gleeble system to obtain the thermal-simulated specimens. Because of the thermal inertia, the peak temperature input into the Gleeble system was set with a short holding time about 0.1 s until the specimen actually reached the peak temperature.

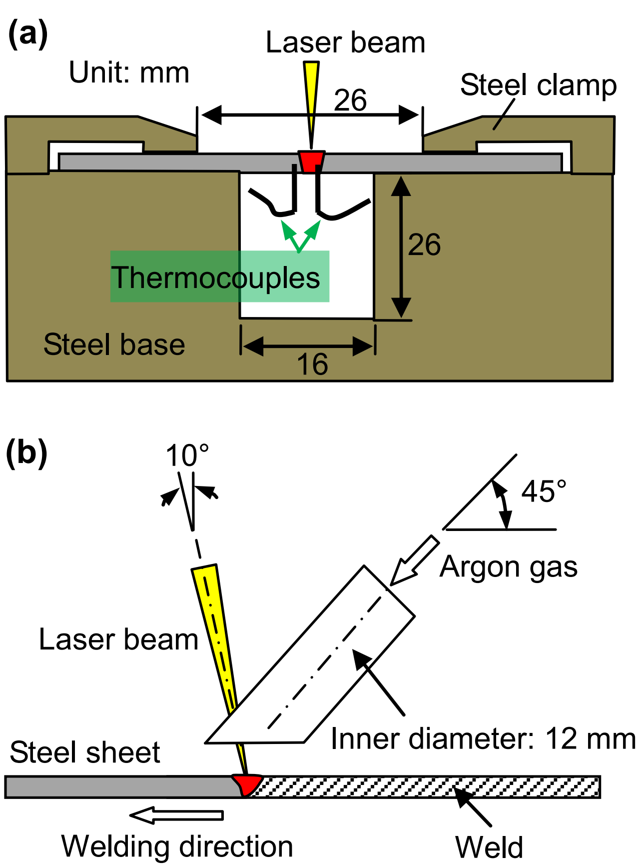

Fig. 1 Schematic diagram of laser welding setup: **a** cross-section view and **b** side view

The maximum heating rate of about 5,000 °C/s was achieved. To realize the rapid cooling, the quenching by 0.6 MPa compressed air was conducted as soon as the peak temperature was reached. This case not only effectively cooled the specimen by the desired cooling rate but also prevented cracking when cooling with water. And the $t_{8/5}$ (the cooling time from 800 to 500 °C) was in the range of 0.4~0.5 s. Finally, thermal-simulated HAZ with the width of about 8 mm was successfully obtained, as shown in Fig. 2.

2.4 Microstructure and mechanical property testing

Cross sections perpendicular to the welding direction of laser-welded joints were mounted, polished, and etched with 4 % nital to observe the microstructure by an optical microscope and a scanning electron microscope (SEM). A two-stage color etching [43], 4 % picral and then 10 % aqueous sodium metabisulfite solution, was used to clearly distinguish between ferrite and martensite. Thus, the volume fraction of martensite f_M was determined by quantitative metallographic techniques. Microhardness testing was also carried out with a Vickers indenter at a load of 200 g and the dwelling time of 15 s. The microhardness was tested along the transverse centerline of the cross section of welded joints.

Uniaxial tensile testing was carried out to obtain the mechanical properties of various specimens. The schematic diagram of various types of specimens is shown in Fig. 3. The specimens of base metal, transverse and longitudinal joints follow the subsize geometry of ASTM E8M standard. The weld specimen with a miniature size was cut from the weld zone directly. The specimens of thermal-simulated HAZ follow a non-standard size (marked as short size in this paper). Tensile testing was operated at a constant crosshead speed of 2 mm/min, and three repetitions were performed for each test. To rule out the effect of specimen size on results, the validity of measured data obtained from the miniature and short size specimens was also confirmed with the same test of the base metal.

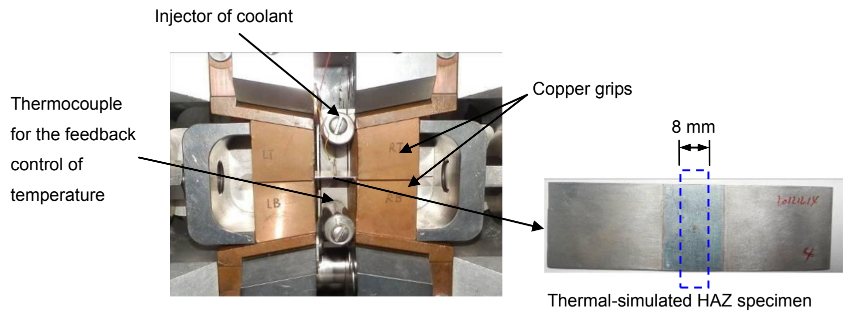

Fig. 2 Experimental setup and thermal-simulated specimen

3 Regional characterization of HAZ properties

3.1 Microstructure and microhardness

The microhardness profile of the DP600 welded joint is shown in Fig. 4. The weld exhibits significantly high microhardness, approximately 1.5 times higher than that of base metal. Most of HAZ has a higher microhardness than base metal, and its microhardness shows a gradual decrease from the fusion line to base metal. However, the softened zone is observed in the HAZ close to base metal, which is mainly due to the local tempering of martensite [44–47]. The softened zone locates at a distance of about 1.2 mm from the weld centerline, which has a width of about 100 μm.

Figures 5 and 6 show the microstructures at different locations in the joint. Different locations of regions are marked individually by their distance (mm) from the weld centerline, i.e., HAZ-0.4 means the location of HAZ having a distance of 0.4 mm away from the weld centerline. As shown in Figs. 5a and 7a, base metal is composed of ferrite (F) with the islands of martensite (M), and the volume fraction of martensite f_M is about 15 %. Weld zone is dominated by the lath martensite along with a small amount of ferrite (Fig. 5b). HAZ shows varied microstructures at different locations: (1) HAZ-0.4 adjacent to the fusion line has a high f_M of 89 %, as shown in Fig. 6a, while the lath martensite grain is finer than that of the weld zone; (2) It can be observed from Fig. 6b–f that f_M decreases sharply with increasing distance from the weld centerline; (3) Little decomposition of martensite grain is observed in HAZ-1.2 (Fig. 7b), i.e., the tempered martensite (TM), which results in the softening. Variations in microhardness at different locations of HAZ are mainly due to the variation of the volume fraction and the size of martensite.

3.2 Measurement of thermal histories

Based on the previous microstructure and microhardness study, eight thermocouples were positioned at different locations in weld and HAZ, as shown in Fig. 8. The thermal histories of weld were also simultaneously measured to investigate the temperature characteristics of the whole joints. Measured thermal histories during laser welding process are shown in Fig. 9. All thermal histories show rapid heating and cooling, which is the characteristic of laser welding process. The interval of the starting time between the two adjacent thermal histories is about 0.12 s, which can infer that the heat source moves a distance of 6 mm in 0.12 s. That is to say, it is corresponding with the actual welding speed of 3 m/min.

As shown in Fig. 9, the difference in locations causes a significant difference in peak temperature, and the peak temperatures decrease with increasing distance from the weld centerline. The temperature of the welding pool reaches above

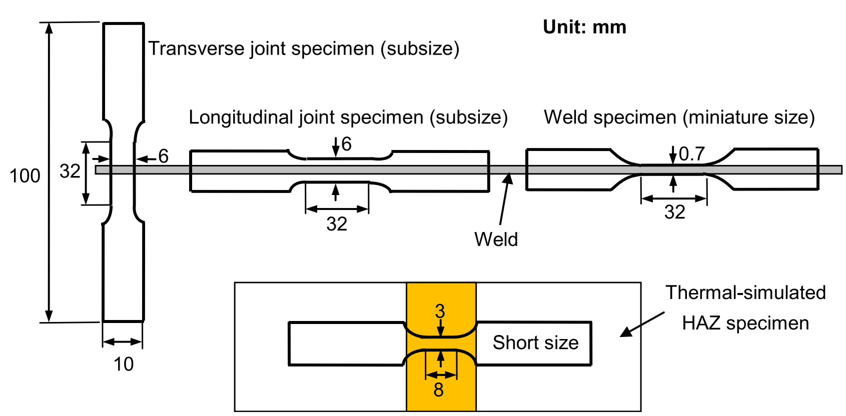

Fig. 3 Schematic diagrams of tensile testing specimens

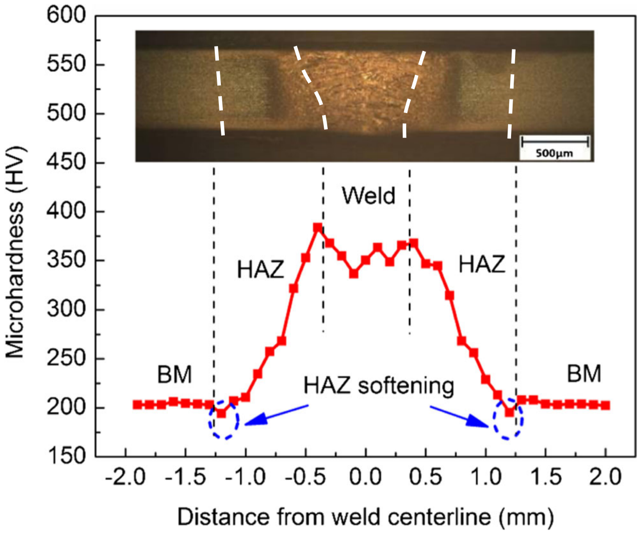

Fig. 4 Microhardness profile of laser-welded DP600 joint

1,600 °C with extremely high heating rate (~10^5 °C/s), exceeding the melting point of base metal (1,530 °C). The peak temperature of HAZ is in the range of 1,360–733 °C varying with locations. The peak temperature of the inner HAZ (HAZ close to weld) is more susceptible to location than that of the outer HAZ (HAZ close to base metal). For instance, the temperature difference between HAZ-0.35 and HAZ-0.55 is 349 °C. However, the difference between HAZ-0.7 and HAZ-1.2 is 200 °C. Consequently, microhardness and microstructure of the inner HAZ are more susceptible to location than those of the outer HAZ, as shown in Figs. 4 and 6, respectively. HAZ-1.2 is located in the softened zone, and its peak temperature is 733 °C and slightly higher than A_{c1}= 718 °C calculated by Andrews's formula [48].

However, the cooling rate does not show such location susceptibility, as shown in Fig. 9. All the $t_{8/5}$ are in the range of 0.303~0.389 s, and the corresponding cooling rate is in the range of 771~990 °C/s. This cooling rate is much higher than 120 °C/s, the critical cooling rate for the martensite formation of DP600 base metal [46]. Hence, the martensitic transformation occurs in the weld and HAZ under such rapid cooling rate.

3.3 Thermal simulation of HAZ

Considering the location susceptibility of thermal histories, microstructure, and microhardness, five typical thermal-simulated HAZ regions were selected: (1) HAZ-0.4, in the coarse-grained zone adjacent to the fusion line and with a peak temperature of 1,200 °C; (2) HAZ-0.5, in the coarse-grained zone and with a peak temperature of 1, 100 °C; (3) HAZ-0.7, in the fine-grained zone and with a peak temperature of 950 °C higher than A_{c3}=859 °C calculated by Andrews's formula [45]; (4) HAZ-1.0, in the intercritical zone and with a peak temperature of 800 °C between A_{c3} and A_{c1}; (5) HAZ-1.2, in the softened zone and with a peak temperature of 730 °C near A_{c1}. Two HAZ regions, HAZ-0.4 and HAZ-0.5, in the coarse-grained zone were investigated because this zone has a sharp microstructure change. The peak temperatures of HAZ-0.4, HAZ-0.7, and HAZ-1.2 for thermal simulation were the same with the measurement results presented in Fig. 9, while those for HAZ-0.5 and HAZ-1.0 were calculated by the linear interpolation of the peak temperatures of their adjacent two zones.

The setting thermal histories of the five thermal-simulated HAZ regions are demonstrated in Fig. 10. The simulated thermal histories are approximately similar to those of the actual HAZ regions in Fig. 9. They all exhibit rapid heating and cooling, and the peak temperatures are falls in the range of peak temperature of actual HAZ. The microstructures of the thermal-simulated HAZ regions are shown in Fig. 11. It is revealed that the microstructures of the thermal-simulated HAZ regions are comparable with the actual HAZ regions shown in Figs. 6 and 7, respectively.

Microhardness test is also carried out to observe the variations between the actual and the thermal-simulated HAZ regions. This method has also been reported by the researchers

Fig. 5 Microstructures of **a** base metal and **b** the weld zone. *M* and *F* stand for martensite and ferrite, respectively

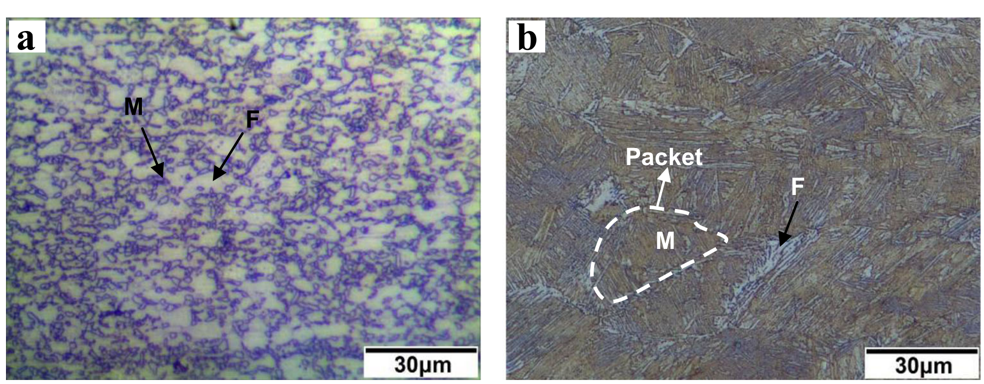

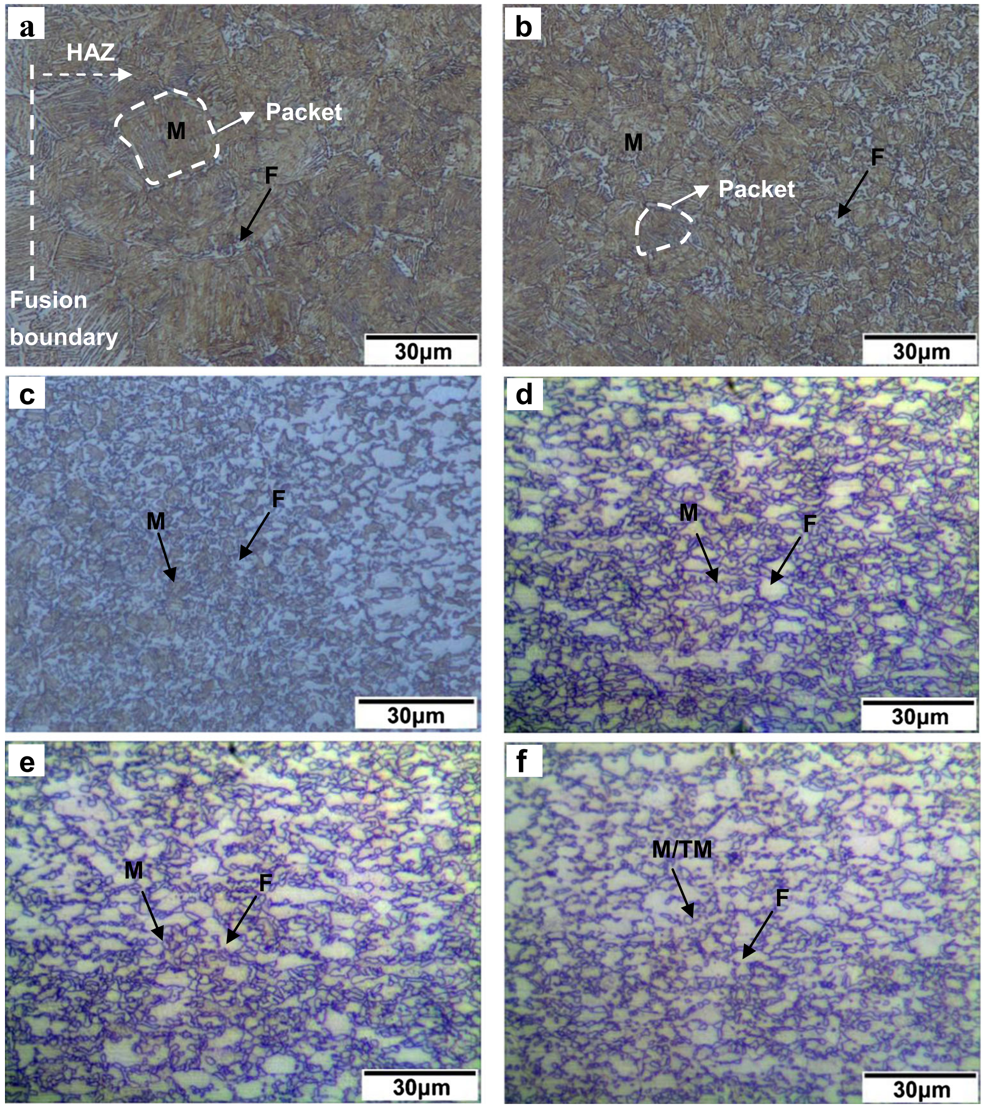

Fig. 6 Microstructures of HAZ at different locations: **a** HAZ-0.4; **b** HAZ-0.5; **c** HAZ-0.8; **d** HAZ-0.9; **e** HAZ-1.0; **f** HAZ-1.2. *TM* stands for the tempered martensite

[41, 49]. As shown in Fig. 12, the microhardness of thermal-simulated HAZ regions has the same gradual tendency with that of actual, and it also nearly falls in the range of the actual HAZ. There is no significant microhardness variation between the actual and thermal-simulated HAZ. Therefore, the microhardness of the thermal-simulated HAZ can reflect of the actual.

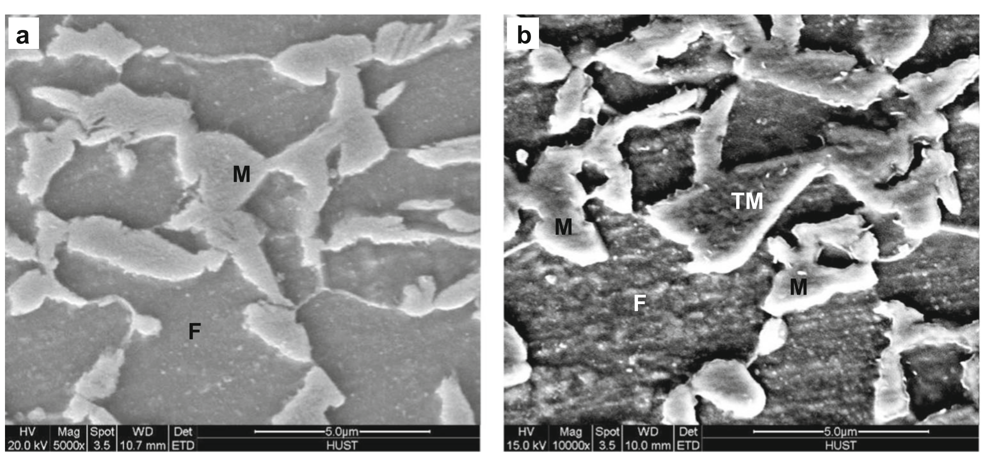

Fig. 7 SEM images of **a** DP600 base metal and **b** the softened zone

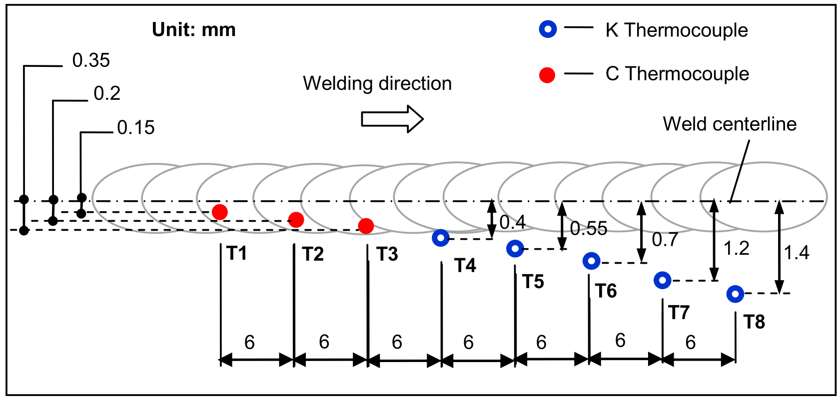

Fig. 8 Locations of different thermocouples

3.4 Evaluation of regional mechanical property

Stress-strain curves of base metal with different specimen geometries were compared to validate the results obtained by non-standard specimens, as shown in Fig. 13. Miniature size and short size specimens both exhibit similar stress-strain curves to that of the standard subsize tensile specimen before failure. Therefore, the short size and the miniature specimens can produce reliable results, and we can rule out the effect of specimen size.

Figure 14 shows the stress-strain curves of weld metal and HAZ regions, and their main mechanical properties are described in Fig. 15. Compared with the base metal and HAZ, the weld metal exhibits the highest strength (1,127 MPa) and the lowest elongation (5.6 %). The strength and elongation of thermal-simulated HAZ fall in between those of base metal and weld metal. And different HAZ regions exhibit significant different mechanical properties. With increasing distance from weld centerline, the strength decreases but the elongation increases. The properties of simulated HAZ-0.4 are very close to simulated HAZ-0.5. Softening is not apparently observed in simulated HAZ-1.2.

The variations in mechanical properties of different regions could be attributed to microstructure change. For low carbon steel with dominated martensite microstructure, the strength increases with increasing the packet size of lath martensite [50]. For low carbon steels with martensite and ferrite microstructure, the strength increases but the elongation decreases, with increasing volume fractions of martensite [51–53]. Three cases of mechanical properties are discussed as follows.

1. For weld zone and the inner HAZ, HAZ-0.4 and HAZ-0.5, they have dominated martensite microstructure and their variation of f_M could be negligible. And thus the packet size of lath martensite plays the most important role in the mechanical properties. Possibly due to the decrease of packet size, the strength of weld zone is higher than the inner HAZ but the elongation is lower. Some typical packets are shown in Figs. 5b, 6a, b. The small variation in mechanical properties of HAZ-0.4 and HAZ-0.5 may be due to the other sub-microstructure of the martensite, such as block and lath [54].
2. For the outer HAZ, HAZ-0.7 and HAZ-1.0, their f_M are not very high; thus, their mechanical properties mainly depend on the f_M. Since the f_M decreases with increasing

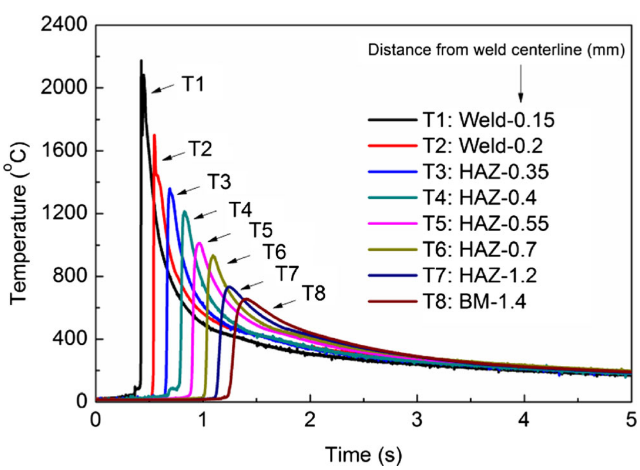

Fig. 9 Thermal histories of different locations during laser welding of DP600 steels

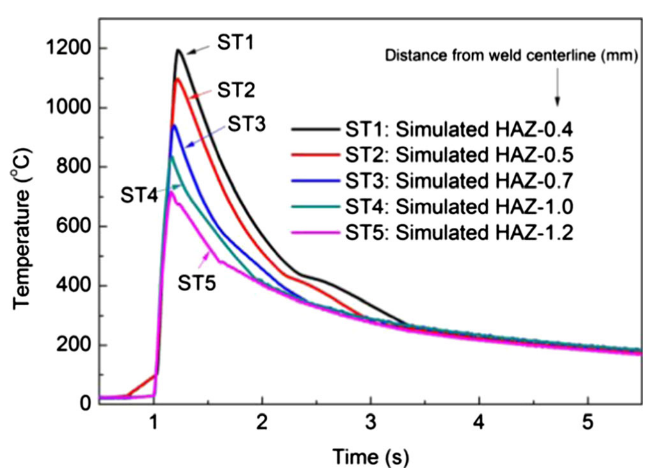

Fig. 10 Thermal histories setting for the thermal-simulated HAZ regions

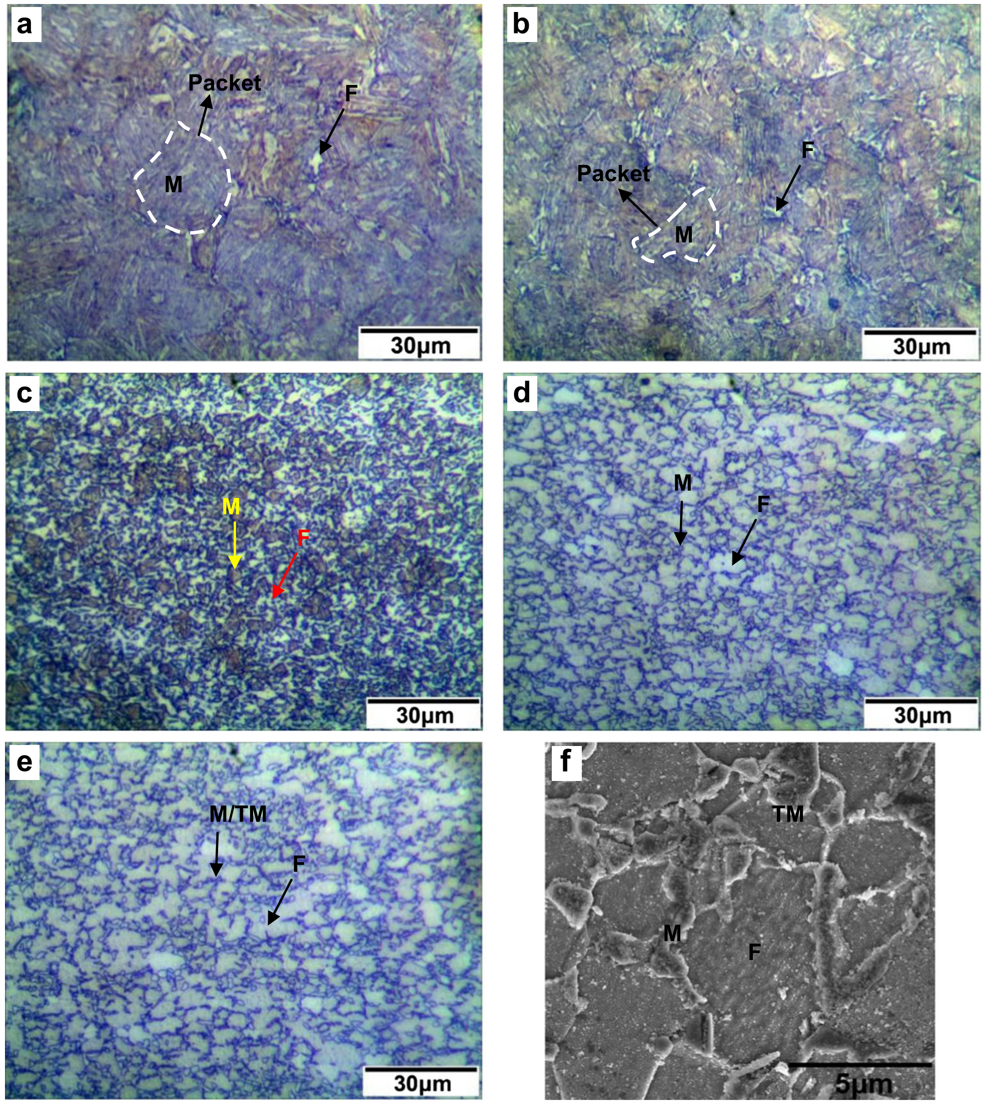

Fig. 11 Microstructures of thermal-simulated HAZ regions: **a** HAZ-0.4; **b** HAZ-0.5; **c** HAZ-0.7; **d** HAZ-1.0; **e** HAZ-1.2; and **f** SEM of HAZ-1.2

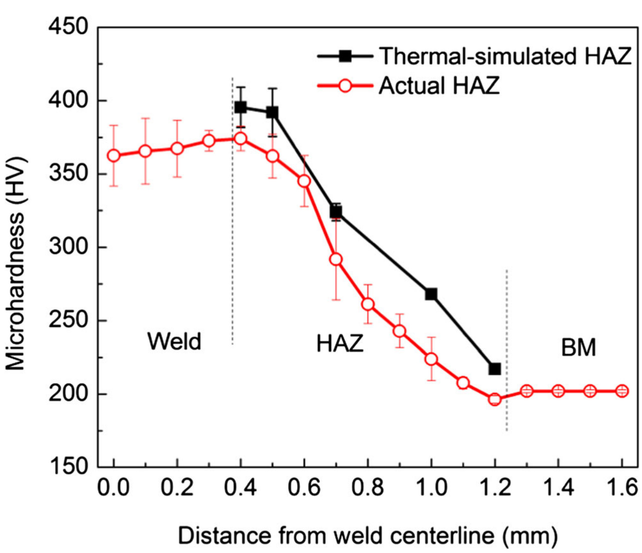

Fig. 12 Microhardness of thermal-simulated HAZ and the actual HAZ

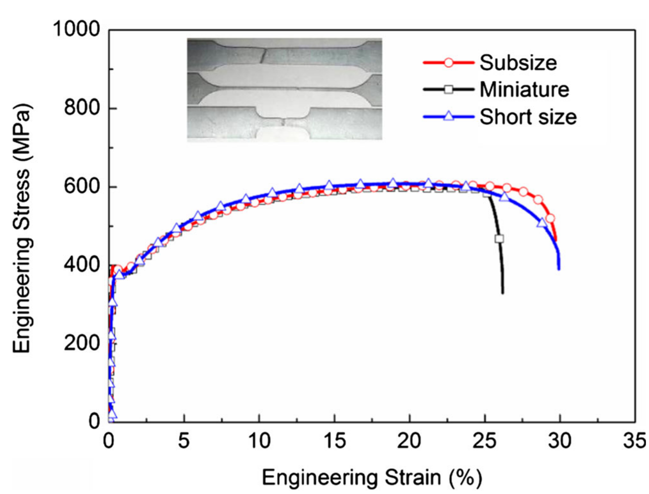

Fig. 13 Stress-strain curves of base metal obtained from subsize, miniature, and short size specimens

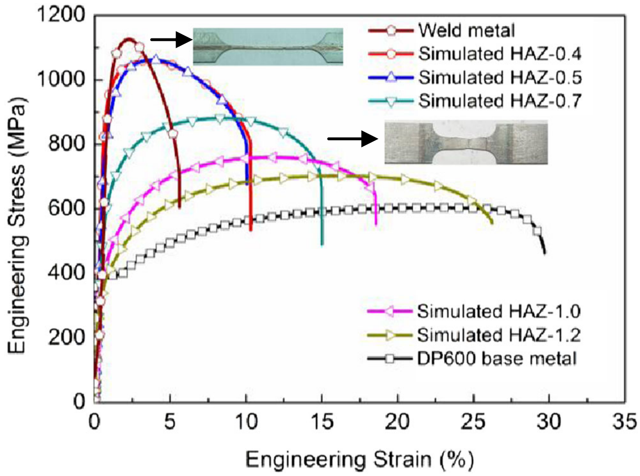

Fig. 14 Stress-strain curves of thermal-simulated HAZ regions and weld metal

distance from weld centerline, the strength decreases but the elongation increases.

3. For softened HAZ, HAZ-1.2, it does not show lower strength and higher elongation. This could be attributed to the ageing of ferrite [49]. Both the aging in the ferrite phase and the tempering in the martensite attribute to the mechanical properties of dual phase steel [55]. In this study, since the small amount of martensite in DP600 base metal, the ageing of ferrite may have more significant effect on mechanical properties than the little tempering of martensite.

4 Numerical modeling based on the regional HAZ properties

4.1 Development of FE model

Numerical modeling of the uni-axial tensile test was performed on both transverse and longitudinal joints to validate the mechanical properties of HAZ regions. Three-dimensional FE model was established based on the ABAQUS/Standard implicit code. The eight-noded linear solid elements with the reduced integration (C3D8R) were used for all joints. The modeled joint geometries are similar with the experimental shown in Fig. 3.

Figure 16 shows the FE meshing and boundary condition, detailing the regions with different mechanical properties and their widths. HAZ was divided into five regions, corresponding with the regional properties characterization in Section 3.4. The element size was approximately 0.2 mm×0.2 mm for base metal and weld zone, and 0.1 mm×0.1 mm for HAZ regions. As shown in Fig. 16, the deformation of joint was motivated by one end of joint with a constant velocity of 2 mm/min, while the other end was fixed. This boundary condition was consistent with the experimental.

The mechanical properties of each HAZ region, as well as the weld and base metal, were considered to be isotropic and homogeneous. Their deformation was governing by their elastic-plastic constitutive behavior (or the true stress-strain curve). Both the elastic and the plastic true stress-strain curves were calculated by the experimental engineering stress-strain curves in Fig. 13. For all regions, the elastic material

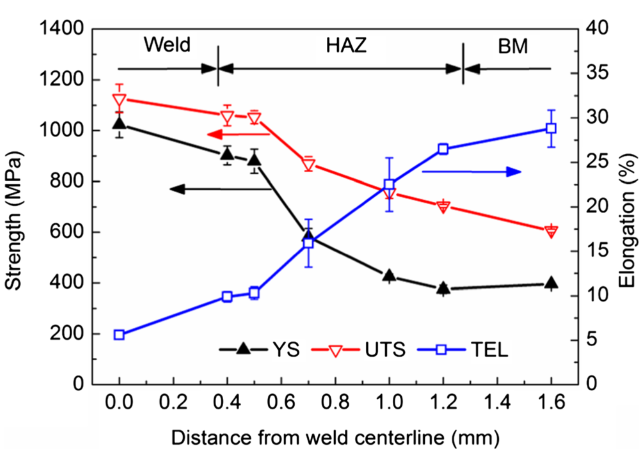

Fig. 15 Mechanical property distribution across the joint

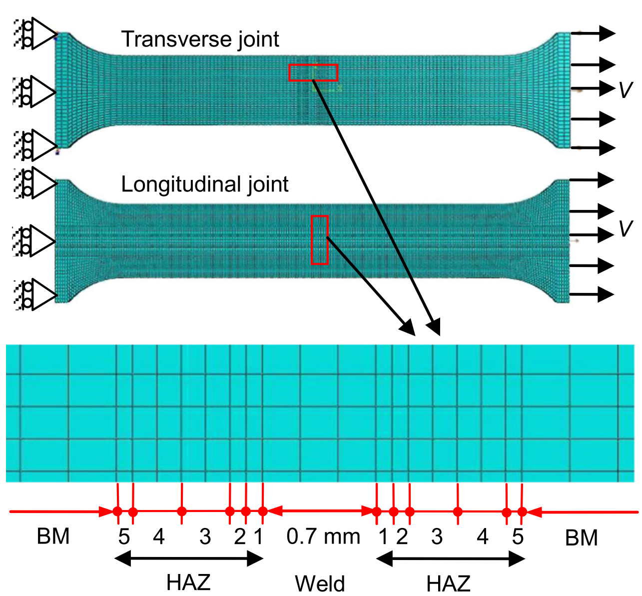

No.	Zone of which mechanical property is assigned	Width (mm)
1	HAZ-0.4	0.1
2	HAZ-0.5	0.1
3	HAZ-0.7	0.3
4	HAZ-1.0	0.3
5	HAZ-1.2	0.1

Fig. 16 Meshing of welded joints and the boundary condition

properties were determined by elastic modulus of 210 GPa and the Poisson's ratio of 0.3. The plastic part of the true stress-strain curve was assigned the calculated data from the engineering stress-strain curves based on Eq. (1).

$$\begin{array}{l}\sigma_T = \sigma_E(1+\varepsilon_E) \\ \varepsilon_T = \ln(1+\varepsilon_E)\end{array}, \quad (1)$$

where, σ_E, σ_T, ε_E, and ε_T are the engineering stress, the true stress, the engineering strain, and the true strain, respectively.

4.2 Validation of the FE model

The simulation and the experimental results are both included in Fig. 17. The simulated necking locations show good agreement with the experimental failure locations. For the transverse joints, the failure occurs at the base metal, which means HAZ softening does not seriously influence the mechanical properties of the transverse joint. This may be due to the low softening of DP600 base metal. For the longitudinal joint, failure initiates at the weld, and this is caused by the low ductility of weld compared with the base metal and HAZ.

In order to investigate the contribution of HAZ to the joint performance, two kinds of welded joint in FE model are compared, i.e., joint-WH (joint including base metal, weld, and HAZ), joint-WO (joint including only base metal and weld, treating HAZ as base metal). Figure 18 shows simulated engineering stress-strain curves. In Fig. 18a, there is no obvious difference between the stress-strain curves of the transverse joint-WH and the transverse joint-WO because base metal undergoes most of the deformation. The simulated stress-strain curves agree well with the experimental results.

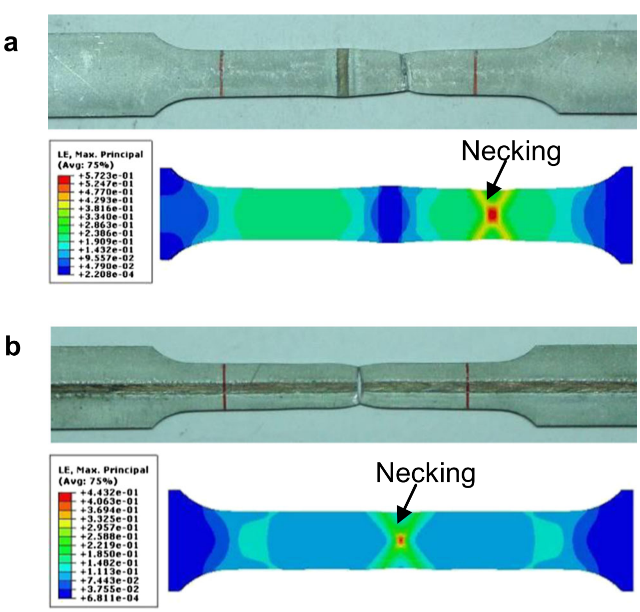

Fig. 17 Experimental and simulated results for tensile tests of **a** the transverse joint and **b** the longitudinal joint

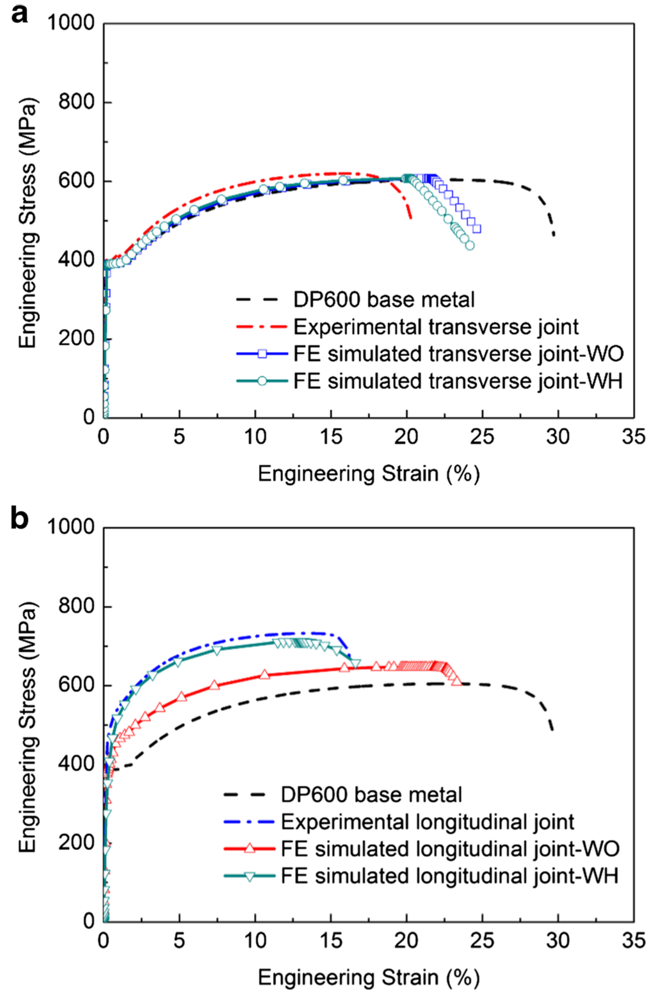

Fig. 18 Experimental and simulated engineering stress-strain curves of **a** transverse joint and **b** longitudinal joint

In Fig. 18b, the stress-strain curve of the longitudinal joint-WH shows better agreement with the experimental than that of the longitudinal joint-WO. This reveals that the regional HAZ properties in the model are very important to the accurate prediction of the whole welded joint performance.

5 Conclusions

Regional mechanical properties of HAZ are investigated by the thermal simulation based on the measured thermal histories and are applied in the numerical model of tensile testing of welded joint. The main conclusions are as follows.

1. The thermal histories in HAZ show rapid heating and cooling rates and significant location susceptibility. The peak temperature decreases sharply with increasing distance from the weld centerline, in the range of about 1, 360~730 °C. The cooling rate ($t_{8/5}$) does not show quite

difference in weld and HAZ, around 0.30 to 0.39 s. The thermal histories result in the location susceptibility in microstructure because the volume fraction of martensite decreases sharply with increasing distance from the weld centerline.

2. The mechanical properties of HAZ regions show that the strength decreases with increasing distance from weld centerline but the elongation increases. The reason is mainly that the packet size of lath martensite and the volume fractions of martensite decrease with increasing distance from the weld centerline. The strength of softened HAZ is slightly higher than that of base metal, and this is possibly because the ageing of ferrite has more significant effect on the mechanical properties than little tempering of martensite.
3. Based on the regional mechanical properties of HAZ, the numerical simulations for the tensile properties of welded joints show good agreement with the experiments, and this can improve the prediction accuracy of laser-welded joint performance.

Acknowledgments The authors gratefully acknowledge the sponsorship and technical supports from GM China Science Laboratory and the State Key Laboratory of Materials Processing and Die & Mould Technology in Huazhong University of Science Technology (HUST). Authors appreciate the kind help from Prof. Chunming Wang and Mr. Xiyuan Hu for the laser-welding experiments. Thanks are also given to the Center for Nanoscale Characterization and Devices, Wuhan National Laboratory for Optoelectronics (WNLO), and the Analytical and Testing Center in HUST for the analytical and testing services.

References

1. American Iron and Steel Institute (1999) UltraLight steel auto body final report
2. Assunção E, Quintino L, Miranda R (2010) Comparative study of laser welding in tailor blanks for the automotive industry. Int J Adv Manuf Technol 49:123–131
3. He S, Wu X, Hu SJ (2003) Formability enhancement for tailor-welded blanks using blank holding force control. J Manuf Sci Eng 125:461–467
4. Abbasi M, Hamzeloo SR, Ketabchi M, Shafaat MA, Bagheri B (2014) Analytical method for prediction of weld line movement during stretch forming of tailor-welded blanks. Int J Adv Manuf Technol 73:999–1009
5. Chan LC, Cheng CH, Chan SM, Lee TC, Chow CL (2005) Formability analysis of tailor-welded blanks of different thickness ratios. J Manuf Sci Eng 127:743–751
6. Abbasi M, Bagheri B, Ketabchi M, Haghshenas DF (2012) Application of response surface methodology to drive GTN model parameters and determine the FLD of tailor welded blank. Comput Mater Sci 53:368–376
7. Panda SK, Kumar DR (2009) Study of formability of tailor-welded blanks in plane-strain stretch forming. Int J Adv Manuf Technol 44: 675–685
8. Panda SK, Sreenivasan N, Kuntz M, Zhou Y (2008) Numerical simulations and experimental results of tensile test behavior of laser butt welded DP980 steels. J Eng Mater Technol Trans 130:0410031–0410039
9. Sreenivasan N, Xia M, Lawson S, Zhou Y (2008) A comparative study of formability of diode laser welds in DP980 and HSLA steels. J Eng Mater Technol Trans 130:0410041–0410049
10. Sharma RS, Molian P, Des M (2009) Yb:YAG laser welding of TRIP780 steel with dual phase and mild steels for use in tailor welded blanks. Mater Des 30:4146–4155
11. Narayanan R, Narasimhan K (2006) Weld region representation during the simulation of TWB forming behavior. Int J Form Process 9:491–518
12. Zhao KK, Chun BK, Lee JK (2001) Finite element analysis of tailor-welded blanks. Finite Elem Anal Des 37:117–130
13. Raymond S, Wild P, Bayley C (2004) On modeling of the weld line in finite element analyses of tailor-welded blank forming operations. J Mater Process Technol 147:28–37
14. Bhagwan AV, Kridli GT, Friedman PA (2002) Influence of weld characteristics on numerically predicted deformation behavior of aluminum tailor welded blanks. Finite Elem Anal Des 0386:1–7
15. Panda SK, Kuntz ML, Zhou Y (2009) Finite element analysis of effects of soft zones on formability of laser welded advanced high strength steels. Sci Technol Weld Join 14:52–61
16. Ahmed E, Reisgen U, Schleser M, Mokrov O (2013) Biaxial behavior of laser welded DP/TRIP steel sheets. Int J Adv Manuf Technol 68:1075–1082
17. Chung KH, Lee W, Kim JH, Kim C, Park SH, Kwon D, Chung K (2009) Characterization of mechanical properties by indentation tests and FE analysis–validation by application to a weld zone of DP590 steel. Int J Solids Struct 46:344–363
18. Kim J, Kim YW, Kang BS, Hwang SM (2004) Finite element analysis for bursting failure prediction in bulge forming of a seamed tube. Finite Elem Anal Des 40:953–966
19. Çam G, Erim S, Yeni C, Koçak M (1999) Determination of mechanical and fracture properties of laser beam welded steel joints. Weld Res 6:193–201
20. Ambriz RR, Chicot D, Benseddiq N, Mesmacque G, Torre SD (2011) Local mechanical properties of the 6061-T6 aluminium weld using micro-traction and instrumented indentation. Eur J Mech A Solid 30: 307–315
21. Mark AF, Francis JA, Dai H, Turski M, Hurrell PR, Bate SK, Kornmeier JR, Withers PJ (2012) On the evolution of local material properties and residual stress in a three-pass SA508 steel weld. Acta Mater 60:3268–3278
22. Saunder FI, Wagoner RH (1996) Forming of tailor-welded blanks. Metall Mater Trans A 27:2605–2616
23. Abdullah K, Wild PM, Jeswiet JJ, Ghasempoor A (2001) Tensile testing for weld deformation properties in similar gage tailor welded blanks using the rule of mixtures. J Mater Process Technol 112:91–97
24. Lee W, Chung KH, Kim D, Kim J, Kim C, Okamoto K, Wagoner RH, Chung K (2009) Experimental and numerical study on formability of friction stir welded TWB sheets based on hemispherical dome stretch tests. Int J Plast 25:1626–1654
25. Zhang XP, Darn L (1998) Estimation of the local mechanical properties of pipeline steels and welded joints by use of the microshear test method. Int J Press Vessel Pip 75:37–42
26. Zhan M, Du H, Liu J, Ren N, Yang H, Jiang H, Diao K, Chen X (2010) A method for establishing the plastic constitutive relationship of the weld bead and heat-affected zone of welded tubes based on the rule of mixtures and a microhardness test. Mater Sci Eng A 527: 2864–2874
27. Song YL, Hua L, Chu DG (2012) Characterization of the inhomogeneous constitutive properties of laser welding beams by the micro-Vickers micro hardness test and the rule of mixture. Mater Des 37: 19–27
28. Reis A, Teixeira P, Duarte JF, Santos A, Rocha AB, Fernandes AA (2004) Tailored welded blanks-an experimental and numerical study

in sheet metal forming on the effect of welding. Comput Struct 82: 1435–1442
29. Rojek J, Michalska MH, Bokota A, Piekarska W (2012) Determination of mechanical properties of the weld zone in tailor-welded blanks. Arch Civ Mech Eng 12:156–162
30. Reynolds AP, Duvall F (1999) Digital image correlation for determination of weld and base metal constitutive behavior. Weld J 78:355–360
31. Genevois C, Deschamps A, Vacher P (2006) Comparative study on local and global mechanical properties of 2024 T351, 2024 T6 and 5251 O friction stir welds. Mater Sci Eng A 415:162–170
32. Hatamleh O (2008) Effects of peening on mechanical properties in friction stir welded 2195 aluminum alloy joints. Mater Sci Eng A 492:168–176
33. Brown R, Tang W, Reynolds AP (2009) Multi-pass friction stir welding in alloy 7050-T7451: effects on weld response variables and on weld properties. Mater Sci Eng A 513:115–121
34. Leitao C, Galvao I, Leal RM, Rodrigues DM (2012) Determination of local constitutive properties of aluminium friction stir welds using digital image correlation. Mater Des 33:69–74
35. Farren JD, Hunter AH, Dupont JN, Seidman DN, Robino CV, Kozeschnik E (2012) Microstructural evolution and mechanical properties of fusion welds in an iron-copper-based multicomponent steel. Metall Mater Trans A 43:4155–4170
36. Sutton MA, Yan JH, Avril S, Pierron F, Adeeb SM (2008) Identification of heterogeneous constitutive parameters in a welded specimen: uniform stress and virtual fields methods for material property estimation. Exp Mech 48:451–464
37. Boyce BL, Reu PL, Robino CV (2006) The constitutive behavior of laser welds in 304L stainless steel determined by digital image correlation. Metal Mater Trans A 37:2481–2492
38. Scintilla LD, Tricarico L, Brandizzi M, Satriano AA (2010) Nd:YAG laser weldability and mechanical properties of AZ31 magnesium alloy butt joints. J Mater Process Technol 210:2206–2214
39. Li G, Xu F, Sun G, Li Q (2014) Identification of mechanical properties of the weld line by combining 3D digital image correlation with inverse modeling procedure. Int J Adv Manuf Technol 74:893–905
40. Reisgen U, Schleser M, Mokrov O, Ahmed E (2010) Uni-and bi-axial deformation behavior of laser welded advanced high strength steel sheets. J Mater Process Technol 210:2188–2196
41. Wojnowski D, Oh YK, Indacochea JE (2000) Metallurgical assessment of the softened HAZ region during multipass welding. J Manuf Sci Eng 122:310–315
42. Yang JG, Sung SH, Chen CS, Tan AH (2011) Study of microstructural and mechanical properties of weld heat affected zones of 2024-T3 aluminium using Gleeble simulation. Mater Sci Technol 27:357–365
43. De AK, Speer JG, Matlock DK (2003) Color tint-etching for multiphase steels. Adv Mater Process 161:27–30
44. Furuhara T, Kobayashi K, Maki T (2004) Control of cementite precipitation in lath martensite by rapid heating and tempering. ISIJ Int 44:1937–1944
45. Xia M, Biro E, Tian Z, Zhou YN (2008) Effects of heat input and martensite on HAZ softening in laser welding of dual phase steels. ISIJ Int 48:809–814
46. Hernandez VHB, Nayak SS, Zhou Y (2011) Tempering of martensite in dual-phase steels and its effects on softening behavior. Metal Mater Trans A 42:3115–3129
47. Farabi N, Chen DL, Li J, Zhou Y, Dong SJ (2010) Microstructure and mechanical properties of laser welded DP600 steel joints. Mater Sci Eng A 527:1215–1222
48. Andrews KW (1965) Empirical formulae for the calculation of some transformation temperatures. J Iron Steel Res Inst 203:721–727
49. Dancette S, Massardier-Jourdan V, Fabrègue D, Merlin J, Dupuy T, Bouzekri M (2011) HAZ microstructures and local mechanical properties of high strength steels resistance spot welds. ISIJ Int 51:99–107
50. Morito S, Yoshida H, Maki T, Huang X (2006) Effect of block size on the strength of lath martensite in low carbon steels. Mater Sci Eng A 438:237–240
51. Jiang Z, Lian J, Chen J (1992) Strain hardening behaviour and its relationship to tensile mechanical properties of dual phase steel. Mater Sci Technol 8:1075–1081
52. Sodjit S, Uthaisangsuk V (2012) Microstructure based prediction of strain hardening behavior of dual phase steels. Mater Des 41: 370–379
53. Bag A, Ray KK, Dwarakadasa ES (1999) Influence of martensite content and morphology on tensile and impact properties of high-martensite dual-phase steels. Metal Mater Trans A 30:1193–1202
54. Morito S, Saito H, Ogawa T, Furuhara T, Maki T (2005) Effect of austenite grain size on the morphology and crystallography of lath martensite in low carbon steels. ISIJ Int 45:91–94
55. Waterschoot T, De AK, Vandeputte S, Cooman BCD (2003) Static strain aging phenomena in cold-rolled dual-phase steels. Metal Mater Trans A 34:781–791